



Fluorescence “Turn-off” Sensing of Iron (III) Ions Utilizing Pyrazoline Based Sensor: Experimental and Computational Study

Promila Sharma¹ · Shikha Bhogal¹ · Irshad Mohiuddin² · Mohamad Yusuf¹ · Ashok Kumar Malik¹

Received: 13 June 2022 / Accepted: 2 September 2022 / Published online: 22 September 2022
© The Author(s), under exclusive licence to Springer Science+Business Media, LLC, part of Springer Nature 2022

Abstract

A simple pyrazoline-based “turn off” fluorescent sensor 5-(4-methoxyphenyl)-3-(5-methylfuran-2-yl)-1-phenyl-4,5-dihydro-1*H*-pyrazole (PFM) was synthesized and well characterized by different techniques such as FT-IR, ¹H-NMR, ¹³C-NMR, and mass spectrometry. The synthesized sensor PFM was utilized for the detection of Fe³⁺ ions. Fluorescence emission selectively quenched by Fe³⁺ ions compared to other metal ions (Mn²⁺, Al³⁺, Fe²⁺, Hg²⁺, Cu²⁺, Co²⁺, Ni²⁺, Cd²⁺, Pb²⁺, and Zn²⁺) via paramagnetic fluorescence quenching and showed good anti-interference ability over the existence of other tested metals. Under optimum conditions, the fluorescence intensity of sensor quenched by Fe³⁺ in the range of 0 to 3 μM with detection limit of 0.12 μM. Binding of Fe³⁺ ions to PFM solution were studied by fluorescent titration, revealed formation of 1:1 PFM-Fe metal complex and binding constant of complex was found to be of 1.3 × 10⁵ M⁻¹. Further, the fluorescent sensor has been potentially used for the detection of Fe³⁺ in environmental samples (river water, tap water, and sewage waste water) with satisfactory recovery values of 99–101%.

Keywords Chalcone · Pyrazoline · Fluorescence quenching · Iron · DFT

Introduction

Iron, as one of the most fundamental trace elements, is known for cell formation in the human body system and growth in plants. Ferric ions (Fe³⁺) play an imperative role in lots of critical biological processes (e.g., oxygen transfer in haemoglobin, electron-proton transfer, RNA and DNA synthesis, nerve conduction, enzyme synthesis, and regulation of acid–base balance). However, excess deposition of iron in the human body can cause some severe diseases

including hemochromatosis, Parkinson’s and Alzheimer’s disease, and diabetes [1]. Moreover, the lack of iron in the human body decreases immunity throughout the developmental periods. Subsequently, a trace level of iron plays a vital role in the health of the living organism. Considering importance of evaluation of Fe³⁺ ions concentration, WHO and European legislation have set the permissible limit of iron in drinking water and food as 0.3 ppm (~5.4 μM) and 0.2 ppm (~3.8 μM) respectively [2]. Thus, quantitative detection of Fe³⁺ ion at an ultra-trace level in environmental samples is of prominent concern using efficient analytical methods. Numerous methods (e.g. atomic absorption spectrometry, spectrophotometry, colorimetry, high-performance liquid chromatography, inductively coupled plasma optical emission spectrometry, and electrochemical analysis) for the detection of Fe³⁺ ions have been used with good aspects [3, 4]. However, all these methods emerged with various limitations such as complicated technologies, sophisticated handling, expensive devices, and a long time for operating systems. Therefore, compared with these methods, the fluorescence sensing strategy has gained considerable attention, as it has protruded optimistic method for monitoring and detection of diverse ions in environmental, and biological samples [5]. This consideration is due to a lot of highlights

Highlights

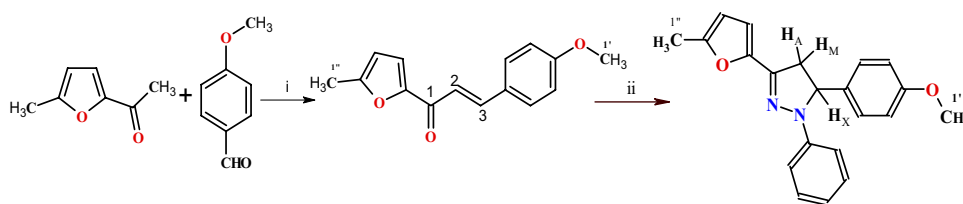
- The PFM exhibits high selectivity and sensitivity towards Fe³⁺ ions over other different metal ions.
- PFM was utilized for the detection of Fe³⁺ in different watersamples (tap, river, and sewage waste water).
- The sensing abilities of PFM towards Fe³⁺ ions were successfully demonstrated by DFT calculations.

✉ Ashok Kumar Malik
malik_chem2002@yahoo.co.uk

¹ Department of Chemistry, Punjabi University, Patiala 147002, Punjab, India

² Department of Chemistry, Punjab University, Chandigarh 160014, Punjab, India

Scheme 1 Synthesis of pyrazoline 5-(4-methoxyphenyl)-3-(5-methoxyfuran-2-yl)-1-phenyl-4,5-dihydro-1*H*-pyrazole



like simplicity, cost-effectiveness, rapid responses, high selectivity, and sensitivity [6].

Pyrazolines derivatives, as the most recent fluorescent sensor have generated much excitement because of their multi-purpose applicability in various fields compared with other fluorescent emitters [7, 8]. The synthetic versatility and the extended synthesis potential of pyrazoline with intrinsic biological and pharmacological activity (e.g. antimalarial, anti-fungal, anti-inflammatory, antibacterial) have made pyrazoline and its derivatives as one of the most well-known precursors to chemistry [9, 10]. Specifically, the assurance of spectroscopic properties of pyrazoline dyes widely used as pH sensors, metal ion fluorescent sensor, living cell imaging probes, and logic-based devices is of great importance [11, 12]. Now a days pyrazolines fluorescence sensors are also contributing in the direction of various other specifications like reusability, reversibility, good quantum yield and suitable fluorescence life time in addition to high sensitivity and selectivity [13–16].

In this context, and in continuation of our research on pyrazoline based fluorescent sensors [17], we synthesized and characterized a “turn Off” fluorescent sensor, namely, 5-(4-methoxyphenyl)-3-(5-methylfuran-2-yl)-1-phenyl-4,5-dihydro-1*H*-pyrazole (PFM). This molecule, detects Fe^{3+} via the paramagnetic enhanced quenching mechanism and offers several advantages such as easy synthesis, high sensitivity and selectivity, and rapid fluorescence quenching response to Fe^{3+} over other metal cations (Al^{3+} , Fe^{3+} , Fe^{2+} , Mn^{2+} , Cu^{2+} , Co^{2+} , Hg^{2+} , Ni^{2+} , Cd^{2+} , Pb^{2+} , and Zn^{2+}). Besides, the DFT calculations were used to confirm the experimental results.

Experimental

Reagents and Measurements

All the metal salts and 4-methoxybenzaldehyde were purchased from Loba Chemie Pvt. Ltd. (Mumbai, India). 2-acetyl-5-methylfuran and phenyl-hydrazine were purchased from Sigma-Aldrich (Mumbai, India). The synthesized compounds were characterized by FT-IR, $^1\text{H-NMR}$, $^{13}\text{C-NMR}$, and mass spectrometry. FT-IR spectra were scanned on a Perkin Elmer Spectrum Infrared Spectrophotometer Version (10.6.0), Japan. $^1\text{H-NMR}$ and $^{13}\text{C-NMR}$ spectra were recorded on a 500 MHz Bruker spectrometer,

Switzerland. LC–MS Spectrometer Model Q-ToF Micro Waters was used to record the mass spectrum of the PFM. To record absorption spectra of the compounds, UV-1800 Shimadzu UV–Visible spectrophotometer (Shimadzu, Japan) was used. All fluorescence experiments were performed with a Shimadzu RF-5301PC spectrophotofluorometer, (Shimadzu, Japan). Triply distilled water (TDW) was used for the experimental work.

Synthesis and Characterization of 5-(4-methoxyphenyl)-3-(5-methylfuran-2-yl)-1-phenyl-4,5-dihydro-1*H*-pyrazole (PFM)

The synthesis of pyrazoline derivative PFM is presented in Scheme 1. The starting material chalcone (CFM) was synthesized from 2-acetyl-5-methylfuran and 4-methoxybenzaldehyde as reported in the literature [18]. Then, a mixture of chalcone CFM (2.42 g, 0.01 mol), phenylhydrazine (1.5 g, 0.01 mol), KOH (0.5 g, 0.01 mol), and ethanol (20.0 ml) was refluxed continuously for 6 h and reaction progress was monitored by TLC. After reaction completion, the resulting mixture was neutralized with iced-HCl to yield a dark brown solid mass. Then, the product PFM was recrystallized from MeOH [19].

Dark Brown solid; Yield: 72%; m.p. 179–180 $^{\circ}\text{C}$; FT-IR: ν_{max} (cm^{-1}): 3100 (aromatic C-H) & 1595 (C=N); $^1\text{H-NMR}$ (500 MHz, CDCl_3): δ 7.17 (4H, m), 7.03 (2H, m), 6.80 (2H, d), 6.73 (1H, d), 6.37 (1H, d), 6.00 (1H, d), 5.11 (1H, dd, $J_{\text{XM}} = 12$ Hz, $J_{\text{XA}} = 7$ Hz, H-X), 3.74 (3H, s, 1'-OCH $_3$), 3.66 (1H, dd, $J_{\text{MX}} = 12$ Hz, $J_{\text{MA}} = 17$ Hz, H-M), 2.97 (1H, dd, $J_{\text{AX}} = 7$ Hz, $J_{\text{AM}} = 17.0$ Hz, H-A), 2.33 (3H, s, 1''-CH $_3$); $^{13}\text{C-NMR}$ (125 MHz, CDCl_3): δ 159.04, 153.86, 146.63, 144.85, 139.36, 134.40, 128.89, 127.12, 119.04, 114.53, 113.58, 111.013, 107.96, 63.4, 55.27, 43.27, 13.91; Calculated ESI–MS: m/z 332.39 for $\text{C}_{21}\text{H}_{20}\text{N}_2\text{O}_3$.

Analytical Procedure

Stock solutions (1 μM) of metal salts i.e. AlCl_3 , $\text{FeCl}_3 \cdot 6\text{H}_2\text{O}$, $\text{FeCl}_2 \cdot \text{H}_2\text{O}$, MnCl_2 , $\text{CuCl}_2 \cdot 2\text{H}_2\text{O}$, $\text{Co}(\text{NO}_3)_2$, HgCl_2 , NiCl_2 , $\text{Cd}(\text{NO}_3)_2$, $\text{Pb}(\text{NO}_3)_2$, and ZnCl_2 were prepared in triply distilled water. The stock solution of probe PFM (2×10^{-5} M) in methanol: water (1:9, v/v) was prepared.

Investigated the fluorescent behavior of the sensor PFM, the fluorescence excitation and emission wavelength were found to be 350 nm and 484 nm respectively. Afterwards, for selectivity, the absorption and fluorescence spectrum of PFM in the presence of each metal salt was recorded. For the experiment, 100 μL of PFM solution, 100 μL of metal salt was taken in cuvette and then diluted up to 3 ml with triply distilled water. For the better considerations of the quenching behavior of sensor PFM, fluorescence titration was performed in the presence of different concentrations of Fe^{3+} ions (0–3 μM). The limit of detection (LOD) value was obtained from the $3\sigma/K$ (where σ is the standard deviation of the blank solution and K represents the slope of the calibration curve between fluorescent intensity and the Fe^{3+} concentrations).

Binding Measurement's

Job's plot analysis was carried out to identify the binding stoichiometry between sensor PFM and Fe^{3+} ions. The solution of sensor PFM and Fe^{3+} ions were prepared to carry out Job's plot experiments. The plot was constructed from the emission profile by maintaining the sum of the concentration of Fe^{3+} ions and the PFM constant. The fluorescence spectrum was recorded by varying the mole fraction of PFM and Fe^{3+} ions at an excitation wavelength of 350 nm. The emission intensity was plotted against the mole fraction of the Fe^{3+} ions. The molar ratio corresponding to the highest point or inflection point on the Job's plot gives the coordination ratio of the PFM to the Fe^{3+} ions [20]. The association constant of PFM with Fe^{3+} was calculated according to the fluorescence emission intensity data using the modified Benesi–Hildebrand equation:

$$\frac{F_{\min} - F_0}{F - F_0} = \frac{1}{K_a[M]} + 1$$

where, F_0 , F , and F_{\min} are the fluorescence intensities of PFM in the absence of Fe^{3+} ions, at an intermediate concentration of Fe^{3+} ions, and a concentration of complete interaction of Fe^{3+} ions, respectively. K_a is the association constant and $[M]$ represents the concentration of the metal ion (Fe^{3+}) [21, 22].

Computational Study

To gain insight into the structures and fluorescence properties of PFM, before and after the addition of metals, density functional theory (DFT) computations were performed on B3LYP/6-311G(d,p)/LANL2DZ using Gaussian 09 software. The optimized geometrical parameters, net charges on active centres, and energetic of the ground state for intermediate chalcone CFM, the sensor (PFM), and its binding with

iron metal (PFM-Fe) were calculated. The spectral theoretical results of vibration analysis, ^{13}C -NMR, and ^1H -NMR of the ligand molecule were also examined.

Detection of Iron in Water Samples

Different water samples (river water, tap water, and sewage waste water) were used for the practical applicability of synthesized sensor. The river water was collected from the Ghaggar River (Patiala, Punjab, India). The tap water was collected from the chemistry lab (Khalsa College, Patiala) and sewage waste water was taken from the Punjabi University, Patiala (Punjab, India). All the water samples were filtered through a Grade 1 Whatman filter paper (pore size: 11 μm) and nylon-6,6 membrane filter (0.2 μm per 47 mm) before analysis. All the samples were tested with the proposed method before spiking.

Results and Discussion

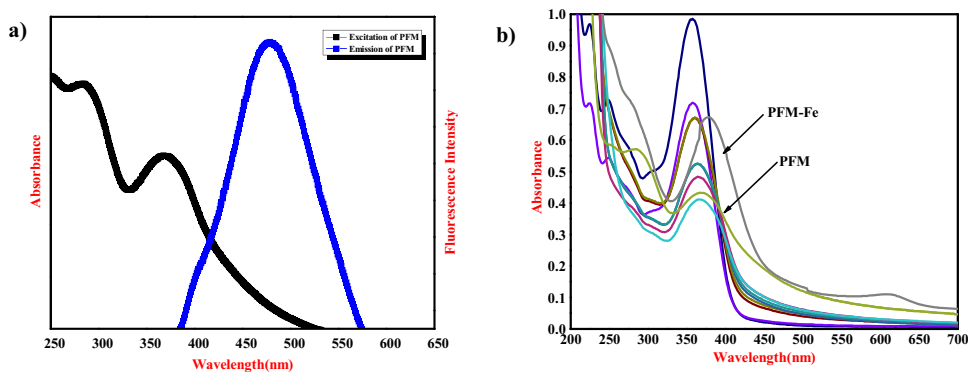
Synthesis and Structural Characterizations

The absence of stretching frequency of α , β -unsaturated carbonyl group and the presence of (C=N) and (C-N) stretching frequencies at 1595 cm^{-1} and 1244 cm^{-1} in the IR-spectrum (Figs. S1 and S2) of the sensor PFM confirmed the subsequent cyclization of chalcone to form the pyrazoline derivative PFM [23]. In the 500 MHz instruments, the ^1H -NMR coupling constant analysis of compound CFM indicated that hydrogen atoms of the olefinic carbon-carbon bond were in a *trans* arrangement ($J = 15$ Hz) (Fig. S3). ^1H -NMR spectra of the compound PFM exhibit the presence of two non-equivalent protons of a methylene group (H_A/H_M) at 2.97 ppm and 3.64 ppm, because of the (H-X) proton at vicinal asymmetric carbon. The methene proton (H-X) appeared as a doublet of doublets at 5.11 ppm, because of vicinal coupling with the two magnetically non-equivalent protons of the methylene group at position 4 of the pyrazoline ring (Fig. S4) [23]. The carbonyl carbon of the chalcone CFM appeared at 177.39 ppm (Fig. S5). A signal due to C=N carbon of the pyrazoline ring was observed in PFM at 159.04 ppm. C4 and C5 carbons of the pyrazoline ring resonated at 63.41 ppm and 43.27 ppm respectively (Fig. S6) [24]. The characteristic peaks of masses were observed at m/z 243.44 (Fig. S7) and m/z 332.39 in the mass spectra of chalcone CFM and ligand PFM (Fig. S8).

Absorption and Fluorescence Experiments of PFM for the Sensing of Fe^{3+} Ion

UV-Vis absorption and fluorescence spectra of compound PFM were presented together in Fig. 1a to determine the

Fig. 1 **a** UV–Vis and Emission spectrum of PFM (2×10^{-5} M) in methanol:water (1:9). **b** UV–Vis spectra of PFM (2×10^{-5} M) in methanol:water (1:9) upon addition of various metal ions (1 μ M)



optical properties of the compound PFM in methanol:water (1:9). The PFM exhibited absorption bands at 286 nm and 366 nm and relatively high intensity fluorescence band at 484 nm. The $n-\pi^*$ transition may be due to conjugation between a lone pair electron of the nitrogen atom in the pyrazoline moiety and the π -bond of the benzene ring.

The effects of several metal ions having biological and ecological importance (Al^{3+} , Fe^{3+} , Fe^{2+} , Mn^{2+} , Cu^{2+} , Co^{2+} , Hg^{2+} , Ni^{2+} , Cd^{2+} , Pb^{2+} , and Zn^{2+}) on the absorption properties of the compound PFM were investigated. For this purpose, solutions having selected metal ions were added into the compound PFM's 2×10^{-5} M aqueous solution. Then absorption measurements of metal ions were realized and recorded in Fig. 1b. Upon addition of metal ions to the solution containing PFM, the band observed at 286 nm diminished while the absorption of the band at 366 nm is enhanced. These changes can be manifest due to charge transfer properties of the pyrazoline moiety [25]. However, in the case of Fe^{3+} ions, the absorption spectra exposed significant changes. A bathochromic shift for band at 366 nm, and a new band at 625 nm was identified. The changes in band position and intensity of several characteristic absorbing peaks in the UV–Vis absorption spectrum of PFM-Fe can be attributed to $n \rightarrow \pi^*$ and $\pi \rightarrow \pi^*$ transitions of the aromatic π system containing the $\text{C}=\text{N}$ bonds [26–28].

Further, to gain insight for the selectivity of sensor PFM, fluorescence measurements were done. Different excitation wavelengths (320–400 nm) were optimized to get the maximum fluorescence emission intensity for PFM. The maximum fluorescence emission intensity (484 nm) was observed at excitation wavelength of 350 nm (Fig. S9). The selective recognition of different metal ions having concentration 1 μ M (Al^{3+} , Fe^{3+} , Fe^{2+} , Mn^{2+} , Cu^{2+} , Co^{2+} , Hg^{2+} , Ni^{2+} , Cd^{2+} , Pb^{2+} , and Zn^{2+}) was examined (λ_{ex} -350 nm; λ_{em} -484 nm). For the selectivity experiment, 100 μ L of different metal solution and 100 μ L of PFM were taken and diluted to 3 mL with TDW. The solution was stirred for 3 min and kept undisturbed at room temperature for 15 min. A large decrease in fluorescence intensity was observed for Fe^{3+} comparative to other metal cations, showing a selective

recognition of Fe^{3+} ion by pyrazoline-based ligand PFM (Fig. 2).

Effect of Response Time

The effect of the response time of the PFM sensor in the presence of Fe^{3+} was investigated at different times (1–20 min). As shown in Fig. S10, the fluorescence intensity of PFM sensor with Fe^{3+} reached equilibrium within 1 min and then almost no change in the fluorescence intensity within 20 min was observed. It showed that PFM quickly coordinates with Fe^{3+} ions in almost 1 min. The rapid and stable response of the sensor PFM could serve as an efficient and consistent probe for Fe^{3+} ions.

Fluorescence Life Time and Quantum Yield

The average lifetime of the PFM sensor in the absence and presence of Fe^{3+} was found to be 1.94×10^{-9} s and 1.55×10^{-10} s respectively. Figure S11 represents the

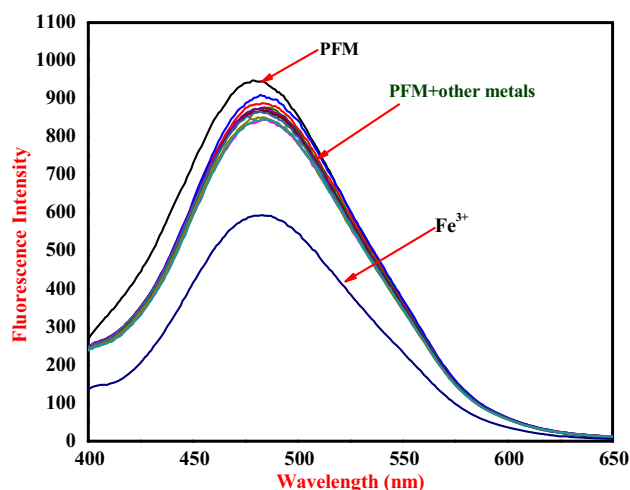


Fig. 2 Fluorescence spectra of PFM (2×10^{-5} M) in methanol:water (1:9) upon addition of various metal ions (1 μ M) (Ex. Wavelength 350 nm)

fluorescence lifetime decay curve of PFM in the absence and presence of Fe^{3+} fitted with three-component exponential decay curve.

The fluorescence quantum yield of the sensor was calculated using quinine sulphate in 0.5 M H_2SO_4 as reference standard. The fluorescence quantum yield of PFM sensor in the absence of Fe^{3+} was measured as 0.69. However, upon the addition of Fe^{3+} , the quantum yield decreases and measured as 0.27.

Reusability and Reversibility

To endorse the reversible and reusability performance of the sensor PFM towards Fe^{3+} ions, the effect of addition of EDTA on the fluorescence was examined. When EDTA was added in to the solution, the fluorescence intensity of compound PFM returned to the earlier state (93%) in which there was no Fe^{3+} ions. This indicates that compound PFM fluorescence sensor system detecting Fe^{3+} ions is reversible and can be reused for further findings. The fluorescence response of subsequent additions of Fe^{3+} or EDTA on PFM was carried out. On adding Fe^{3+} , the fluorescence intensity of PFM decreases while addition of EDTA on PFM increased the fluorescence intensity. These cycles were repeated five times without losing much sensitivity of the sensor (Fig. S12).

Sensitivity Study of PFM for Fe^{3+} Ion

To quantify the sensitivity and fluorescence quenching behavior between PFM and Fe^{3+} , the sensing proficiency

of PFM towards Fe^{3+} was further explored in the range of 0–3 μM . On the addition of Fe^{3+} ions in a sequential manner in the PFM solution, the fluorescence emission intensity of the sensor PFM gradually decreases with the increase in concentration of Fe^{3+} (Fig. 3a). The emission intensity of sensor PFM was specifically quenched by Fe^{3+} ions via paramagnetic fluorescence quenching [5, 29]. The quenching phenomena were further analyzed by the Stern–Volmer equation:

$$\frac{F_0}{F} = 1 + K_{sv} [\text{Fe}^{3+}]$$

where, F_0 is the initial fluorescence intensity of the PFM solution in the absence of Fe^{3+} , F is the fluorescence emission intensity in the presence of Fe^{3+} , and K_{sv} is the Stern–Volmer constant. The Stern–Volmer plot (F_0/F versus $[\text{Fe}^{3+}]$) depicts that the quenching ratio increase linearly with the increase in Fe^{3+} concentration ($R^2=0.99$) (Fig. 3b). The K_{sv} was calculated from the slope of plot and found to be $4.45 \times 10^{-5} \text{ M}^{-1}$.

The limit of detection (LOD) was calculated 0.12 μM for Fe^{3+} using the equation $\text{LOD} = 3\sigma/K$, which are far lower than most extreme toxin levels for Fe^{3+} (5.4 μM) in drinking water given by EPA guidelines (Fig. 3c) [2].

Competitive Selectivity of PFM for Fe^{3+} Ions

To investigate the selectivity and efficiency of PFM towards Fe^{3+} ions, competitive experiment was carried out. For the

Fig. 3 **a** Fluorescence spectra of PFM with increasing concentration of Fe^{3+} ions **b** Stern–Volmer plot for PFM against varying concentrations of iron ions in the range of 0–3 μM **c** Calibration curve of fluorescence intensity of PFM at 484 nm vs. concentration of iron ion excited at 350 nm

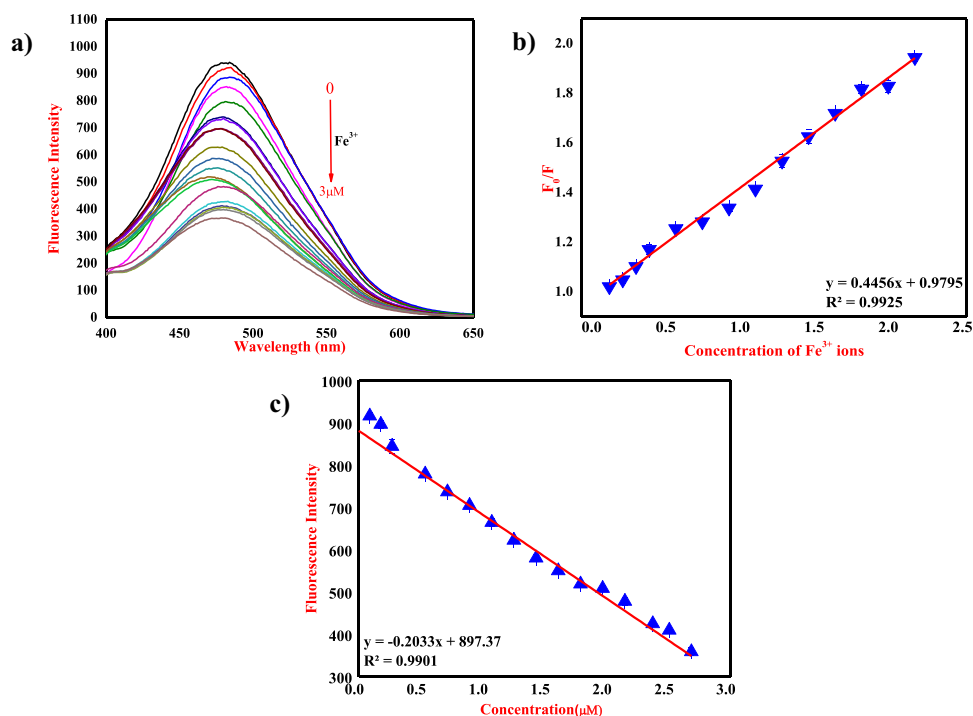
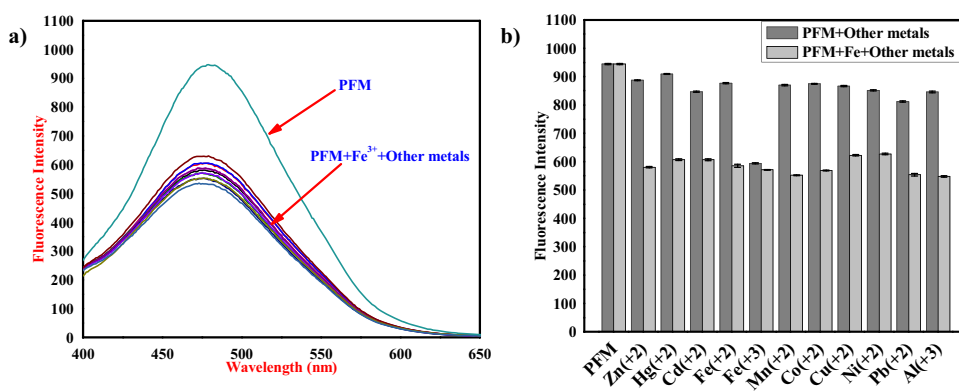


Fig. 4 **a** Fluorescence response of PFM upon addition of Fe^{3+} ion in the presence of other competing metal ions (Ex. Wavelength 350 nm) **b** Dark grey bars represent the fluorescence intensity of PFM in the presence of 1 μM of metal ion. light grey bars represent the fluorescence intensity in the presence of various metal ions after the addition of Fe^{3+}



competitive study, 1 mL of Fe^{3+} (1 μM) was added to the 100 μL of PFM (2×10^{-5} M) solution containing other metal ions (Al^{3+} , Fe^{2+} , Mn^{2+} , Cu^{2+} , Co^{2+} , Hg^{2+} , Ni^{2+} , Cd^{2+} , Pb^{2+} , and Zn^{2+} at concentration of 2×10^{-6} M) were taken and the fluorescence emission spectra was obtained. The interfering metal ions induced no significant changes in the fluorescence intensity of the sensor PFM (Fig. 4). As a result, the PFM can be presented as a highly selective and reliable fluorescent sensor for Fe^{3+} ion recognition [25]. Moreover, relative error (%) for various metal ions was calculated:

$$\text{Relative error (\%)} = [(F - F_0)/F_0] \times 100\%$$

where, F_0 and F are the fluorescence emission intensities in the absence and presence of interfering ion. Table 1 validated the relative error (%) values showing great tolerance of other metals over the Fe^{3+} ion. The relative error is also found to be less than ± 5 . These results suggest that the metal binding of PFM shows an evident preference for ferric ions over other competing ions.

Proposed Binding and Sensing Mechanism

A Job's Plot was performed to calculate the binding stoichiometry of PFM and Fe^{3+} ion (Fig. 5). A turning point at

Table 1 Relative error showing tolerance of other metals

| Interferent ion | Relative Error % ($\Delta F/F_0 \times 100$) |
|------------------|------------------------------------------------|
| Zn^{2+} | 1.411 |
| Hg^{2+} | -1.411 |
| Cd^{2+} | -1.376 |
| Fe^{2+} | 0.882 |
| Mn^{2+} | 4.4107 |
| Co^{2+} | 2.681 |
| Cu^{2+} | -3.0345 |
| Ni^{2+} | -3.493 |
| Pb^{2+} | 4.234 |
| Al^{3+} | 4.869 |

0.5 mol fractions indicates 1:1 metal–ligand binding interactions between sensor PFM and Fe^{3+} . The association constant (K_a) was calculated to be $1.3 \times 10^5 \text{ M}^{-1}$ according to the modified Benesi–Hildebrand equation (Fig. 6).

The mechanism of interaction between the Fe^{3+} and PFM was studied through FT-IR (Fig. S13). It can be proposed that the formation of the coordination between Fe^{3+} and sensor PFM resulted from electronegative atom nitrogen of the pyrazoline ring and the oxygen of the furyl ring (Fig. 7). This interaction causes the fluorescence quenching of the sensor PFM. The FTIR spectrum of PFM exhibits a peak at 1595 cm^{-1} (stretching vibration $\text{C}=\text{N}$), and peak at 1245 cm^{-1} ($\text{C}-\text{O}$ stretching vibration). However, in the PFM- Fe complex, the characteristic stretching vibration $\text{C}-\text{O}$ peak of PFM partially disappear while the $\text{C}=\text{N}$ stretching vibration of pyrazoline ring shifted from to 1595 cm^{-1} to 1561 cm^{-1} . This can be due to the interaction of Fe^{3+} ions with the nitrogen and oxygen atom of PFM. The binding of Fe^{3+} to PFM resulted in the electron or energy transfer from PFM to Fe^{3+} metal ion causes fluorescence quenching of

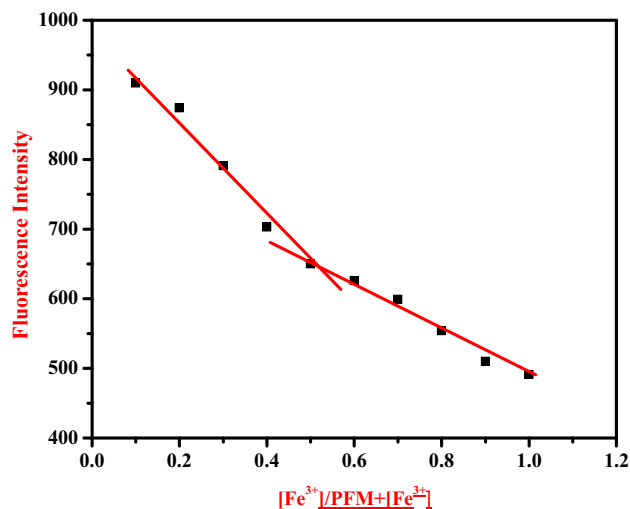


Fig. 5 Job's plot for determining the stoichiometry for PFM and Fe^{3+} ions

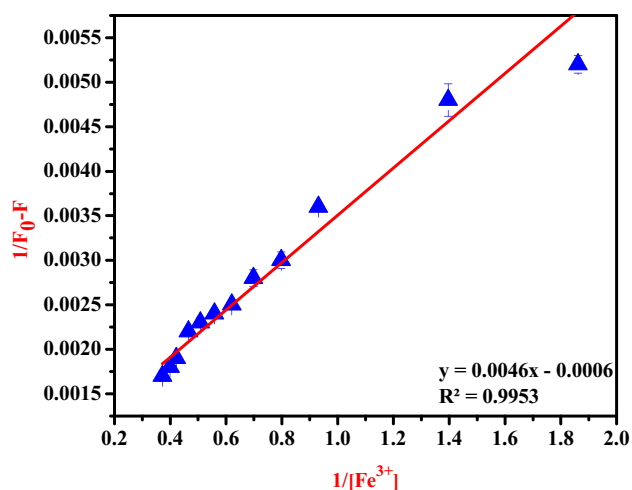


Fig. 6 Benesi–Hildebrand plot (at 350 nm) for complexation of PFM with Fe^{3+} ion

PFM. The fluorescence emission spectra of PFM overlaps with the absorption spectra of Fe^{3+} , suggesting the fluorescence resonance energy transfer (FRET) mechanism for the fluorescence quenching (Fig. S14).

Computational Study

Molecular Geometry Optimization

The optimized structures of these compounds along with the labeling of atoms are shown in Fig. 8. After optimization, the binding energies ($\Delta E = E(\text{complex}) - E(\text{PFM})$) were calculated for all metals with PFM to obtain the strongest binding of the metal cation with PFM. The calculated result, $\Delta E = -564 \text{ kcal mol}^{-1}$ showed the minimum energy changes for iron complex as compared to other metals (Table S1). Also, more negative energy value (-1194.45 a.u.) of the PFM-Fe than the free ligand (-1072.42 a.u.) confirms the stability of the PFM-Fe system compared to other metals showing high selectivity towards iron ions [5, 30, 31].

Also, for chalcone CFM, ligand PFM, and ligand complex (PFM- Fe^{3+}) with iron metal, C–C bond distances are found to be in the range from 1.528–1.533 Å, 1.529–1.539 Å, and 1.531–1.546 Å while for C–N, these values are 1.469 Å, 1.470 Å, and 1.478 Å respectively. In the case of C–H

bond distances, they lie in the range from 1.093–1.103 Å, 1.093–1.101 Å, and 1.092–1.098 Å respectively [30].

Mulliken Population Analysis and Molecular Electrostatic Potential

The Mulliken population analysis is correlated to the vibrational properties and nature of chemical bonds present in the molecule. The Mulliken charge distribution structure and horizontal bar diagram of comparative Mulliken atomic charges of the title compounds are shown in Fig. 9a, b, respectively. All the hydrogen atoms in the compounds carry a net positive charge. The atomic charge distribution shows that the hydrogen atoms of the methoxy group have a bigger positive atomic charge (0.2e to 0.32e) than the other hydrogen atoms. As expected, the charge of the nitrogen atom ($\text{N}31 = -0.1826$, -0.2933 and $\text{N}32 = -0.2574$, -0.2008 in PFM and PFM-Fe respectively) is negative. Additionally, the results illustrate that the charge of the oxygen atoms in the carbonyl group of CFM and furyl ring exhibits a negative charge, which acts as donor atoms. The oxygen atom of $-\text{OCH}_3$ group enforces a large negative charge on the carbon ($\text{C}11 = -0.1285$, $\text{C}26 = -0.3822$, $\text{C}26 = -0.4545$ in CFM, PFM, and PFM-Fe respectively) attached to it. Iron atom ($\text{Fe}46 = 0.7185$) has a high positive charge showing electropositive character.

The electrostatic potential surfaces are correlated with the charge density, shape, dipole moment, and position of chemical reactivity of the molecules. As inspected from the MEPs map of the title compounds (Fig. 10), the negative regions are localized over the electronegative oxygen and nitrogen atoms. The maximum positive regions are localized on the hydrogen atoms and the metal ion [32].

Molecular Reactivity

The electron donor–acceptor properties of various types of molecules can be defined by using the energy of HOMO and LUMO. FMO's also helped to interpret the kinetic stability, charge transfer, and chemical reactivity of a molecule. The frontier molecular orbital distribution of the compounds CFM, PFM, and PFM-Fe were represented in Fig. 11a. The smaller value of the HOMO and LUMO energy gap showed that the studied molecule has high polarizability, chemical reactivity, and biological activity.

Fig. 7 Proposed binding modes of PFM with Fe^{3+} ions

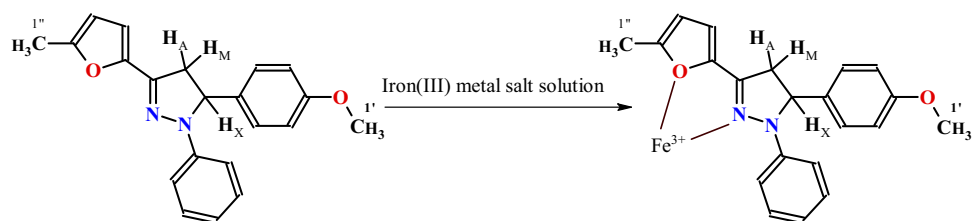
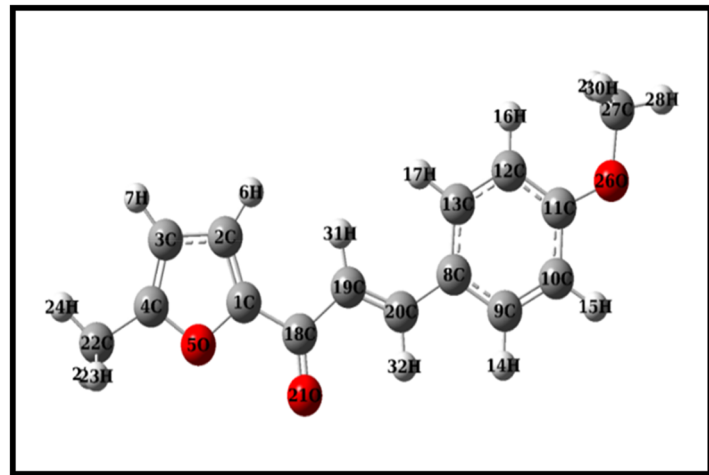
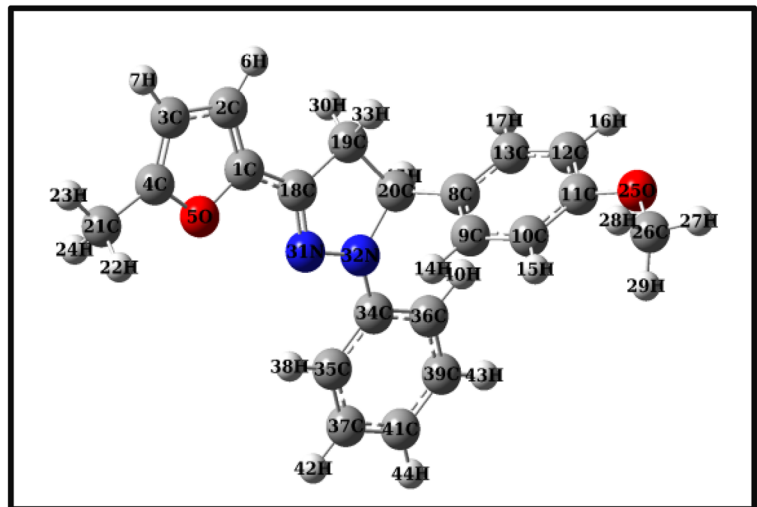


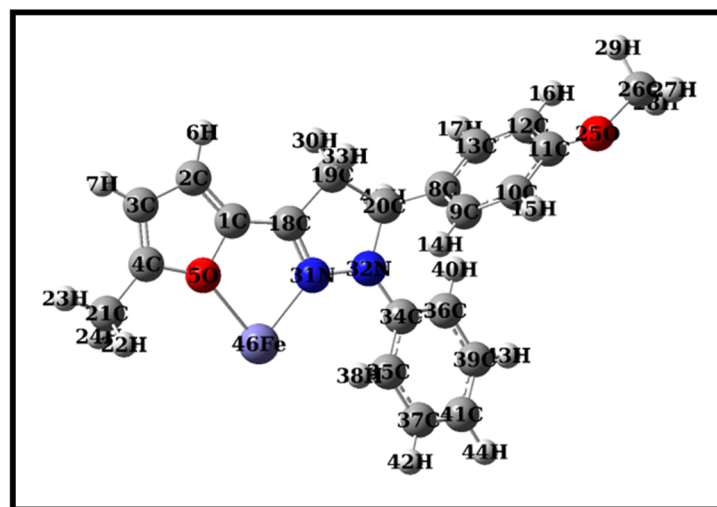
Fig. 8 Optimized geometric structures of CFM, PFM, and PFM-Fe at B3LYP/6-311G (d,p)



CFM



PFM



PFM-Fe

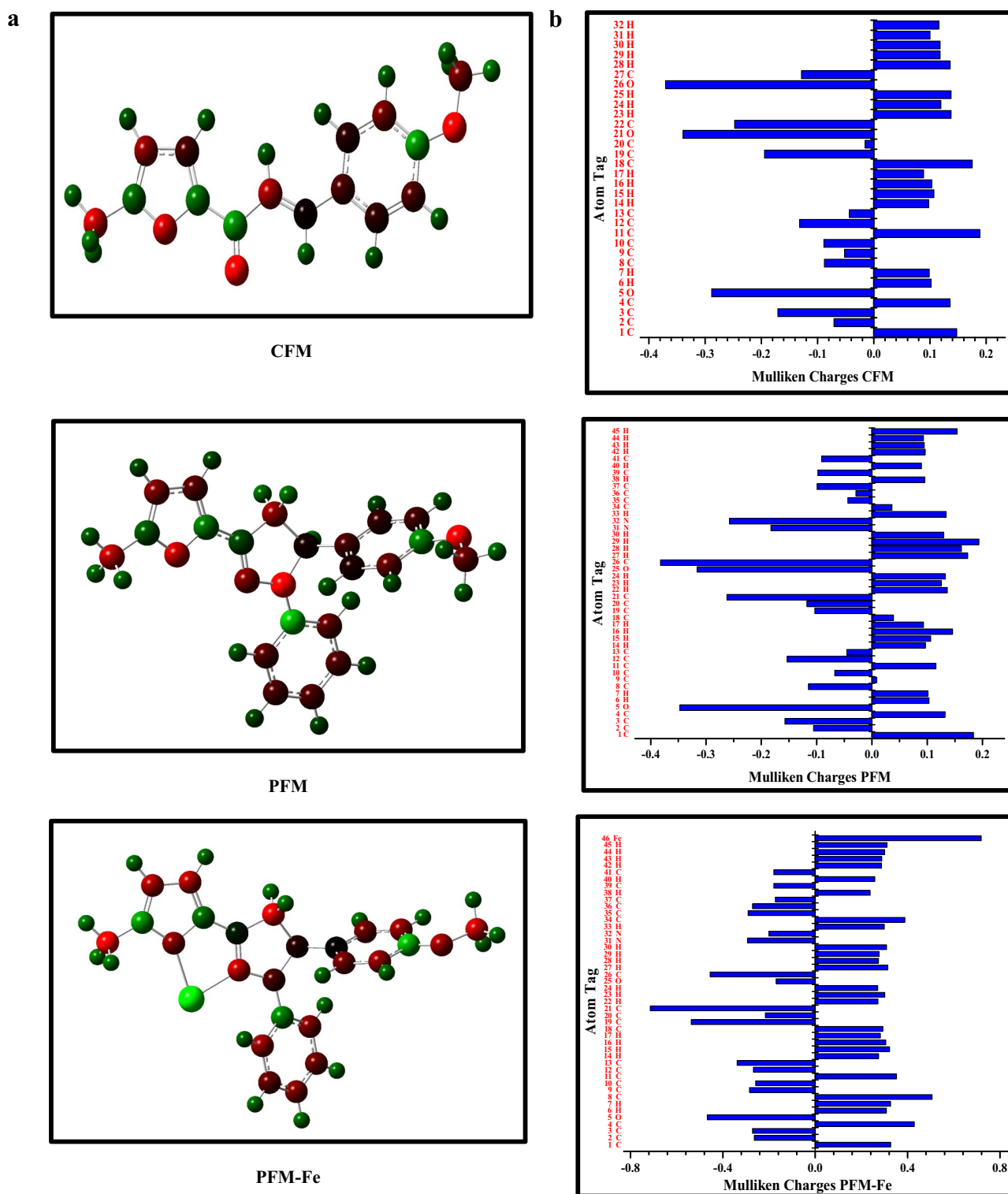


Fig. 9 **a** Mulliken charges of CFM, PFM, and PFM-Fe at B3LYP/6-311G (d,p) **b** Horizontal bar diagram of mulliken atomic charges of title compounds at B3LYP/6-311G(d,p)

In the PFM molecule, the HOMO (−6.621 eV) and the LUMO (−2.506 eV) are situated at the benzene and pyrazoline ring, respectively. For the PFM-Fe, the electron

density of HOMO (−16.079 eV) is mainly situated at the molecular framework. Whereas, the electron density of LUMO (−14.062 eV) is situated at the coordination

Fig. 10 Molecular electrostatic potential (MEPs) of compounds of CFM, PFM, and PFM-Fe at B3LYP/6-311G (d,p) (most electronegative electrostatic potential are red, most positive electrostatic potential are blue and regions close to zero potential are green)

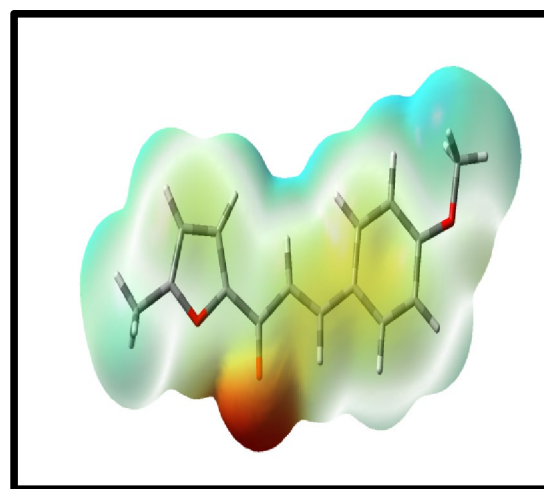
center. The calculated energy gap (Δ) between HOMO and LUMO for PFM-Fe is found to be 2.02 eV, which is lower than that of unbound PFM (4.12 eV). Based on the DFT calculations, the binding between PFM and Fe is energetically favorable. These DFT results implied that the interaction of Fe to PFM effectively decreases the HOMO–LUMO energy gap of the PFM-Fe and intensely stabilizes the sensing of Fe by forming PFM-Fe compound [33]. Furthermore, the chemical reactivity parameters of the compounds (Table 2) were also calculated with the help of the energy of HOMO and LUMO orbitals. Using FMOs energies, the ionization potential (I) and electron affinity (A) can be measured as: $I = -E_{\text{HOMO}}$ and $A = -E_{\text{LUMO}}$.

Moreover, Density of States (DOS) plots of PFM are examined to study the electronic structure of the molecule via population analysis of orbitals. DOS plot represents the energy level of each orbital. DOS plot (Fig. 11b) for PFM shows that FMOs and the energy gap of HOMO–LUMO are in complete agreement with the result obtained from the DFT study [34]. To investigate the optimization process Fig. S15a, a graph displaying deviation from the target was plotted (Fig. S15b). Also, the graph energy vs. optimization step was plotted as shown in Fig. S15c. In these plots, the path of structure convergence was established. As inspected from these plots, the self-consistent field is converging as the line is directed towards zero [35].

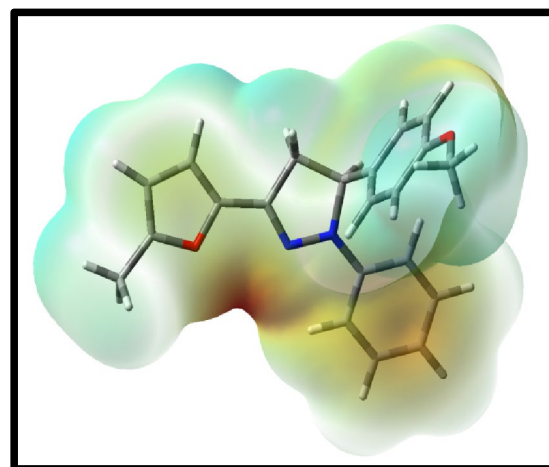
Note: Some other important thermodynamics parameters, NBO, Vibrational analysis, and NMR of the compounds based on theoretical results are discussed in Sect. 1 of the SI.

Detection of Fe^{3+} in Water Samples

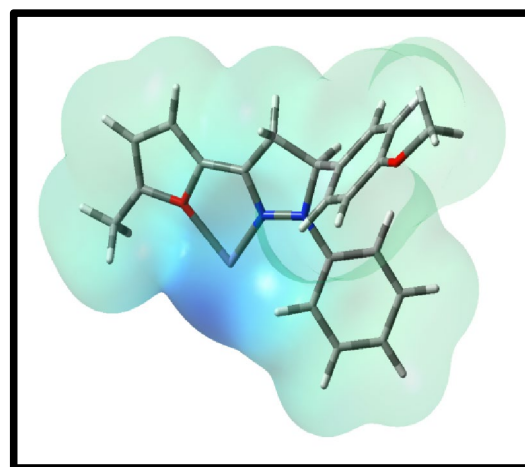
The synthesized PFM sensor was utilized for the detection of Fe^{3+} in different water samples (river water, tap water, and sewage waste water) by using the spike recovery method. All the samples were tested before spiking and the results revealed that the concentrations of Fe^{3+} were either below the LOD or not present in the tested samples. So, all the samples were spiked with different concentrations of Fe^{3+} and the results obtained were shown in Table 3. It can be seen that the detected Fe^{3+} ions concentration is close to the spiked value with a satisfactory recovery value (99.0–101.0%) and low RSD values (0.78–2.03%). This signifies the great practical potential of the present method for the detection of Fe^{3+} in water samples.



CFM



PFM



PFM-Fe

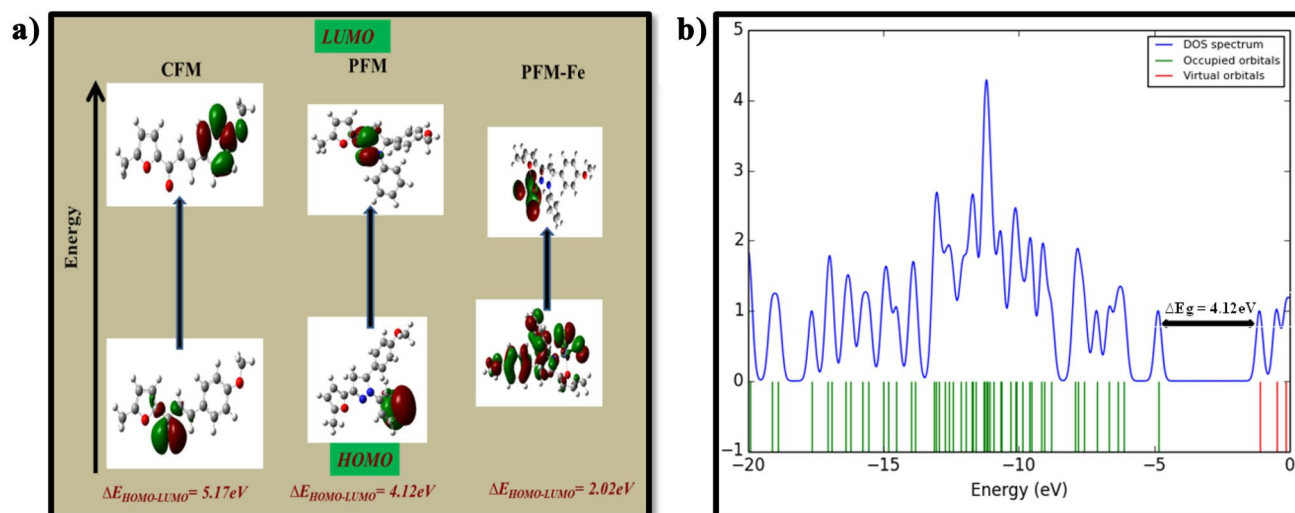


Fig. 11 a FMOs of compounds of CFM, PFM, and PFM-Fe at B3LYP/6-311G (d,p) b Calculated TDOS diagram of PFM using gaussian software

Table 2 Chemical Reactivity Parameters of the Compounds Based on HOMO–LUMO

| S. No | CFM | PFM | PFM-FE |
|--------------------------------------|---------|---------|-----------|
| E_{HOMO} (eV) | -7.308 | -6.6216 | -16.0792 |
| E_{LUMO} (eV) | -2.133 | -2.5064 | -14.0623 |
| $\Delta E_{\text{HOMO-LUMO}}$ (eV) | 5.1747 | 4.11517 | 2.0169 |
| Ionization potential (IP) (eV) | 7.308 | 6.6216 | 16.0792 |
| Electron affinity (EA) (eV) | 2.133 | 2.5064 | 14.0623 |
| Chemical potential (eV) | -4.7207 | -4.564 | -15.07076 |
| Electronegativity (eV) | 4.7207 | 4.564 | 15.07076 |
| Chemical hardness (eV) | 2.5873 | 2.0575 | 1.008454 |
| Chemical Softness (eV) ⁻¹ | 0.1932 | 0.243 | 0.495808 |
| Electrophilic global index (eV) | 4.3065 | 5.0618 | 112.611 |

Table 3 Detection of Fe³⁺ in different water samples (tap, river, and sewage waste water) by the proposed PFM sensor

| Order | Matrix | Amount spiked (μM) | Amount found (μM) | Recovery % | RSD % |
|-------|--------------------|--------------------|-------------------|------------|-------|
| 1 | River water | 0.89 | 0.878 | 98.6 | 0.85 |
| | | 1.79 | 1.77 | 98.8 | 0.91 |
| | | 2.50 | 2.43 | 97.2 | 0.78 |
| 2 | Tap water | 0.89 | 0.884 | 99.3 | 1.23 |
| | | 1.79 | 1.79 | 100.0 | 1.11 |
| | | 2.50 | 2.48 | 99.2 | 2.03 |
| 3 | Sewage waste water | 0.89 | 0.88 | 98.8 | 0.59 |
| | | 1.79 | 1.79 | 100.0 | 0.96 |
| | | 2.50 | 2.50 | 100.0 | 1.20 |

Comparison with Other Reported Fe³⁺ Fluorescent Sensors

To provide quantifiable achievement for the design of a new fluorescent sensor, the sensing performance of PFM was compared with some reported pyrazoline based fluorescent sensors for Fe³⁺ detection (Table 4). As shown in Table 4, the synthesized fluorescent ligand PFM showed a better detection limit for Fe³⁺ (0.12 μM) in comparison to other reported sensors. Pyrazoline based fluorescent sensors such as P [36], Q [37], R [38], and S [39] showed good selectivity for Fe³⁺ ions, but were not used for any real sample analysis. Pyrazole-pyrazoline based sensor (U) [40] showed a better detection limit but the synthetic process was tedious and involved 4 step reaction. On the other hand, the present procedure involves a simple procedure with 2 step reaction (Scheme 1). Moreover, the sensor showed better extraction recovery of 99–101% (tap, river, and sewage waste water) with RSD < 2.1% than the other reported methods.

Table 4 Comparison of sensor PFM with other sensor for detection of iron(III)

| Order | Fluorescent chemosensor | Linear range (μM) | Detection limit (μM) | Recovery % | R.S.D % | Matrix | Ref |
|-------|------------------------------------------------------------------------------------------------------------|--------------------------------|-----------------------------------|------------|-----------|-----------------------------------|------------------|
| 1 | 2-(5-(4-Chlorophenyl)-3-(pyridin-2-yl)-4,5-dihydropyrazol-1-yl) 4 benzo[d]thiazole (P) | 10–200 | 3.0 | | | | [36] |
| 2 | 3-(2,5-dimethylthiophen-3-yl)-5-(9-ethyl-9H-carbazol-3-yl)-4,5-dihydro-1H-pyrazol-1-yl)benzo[d]thiazole(Q) | 10–90 | | | | | [37] |
| 3 | 2-(1-(benzo[d]thiazol-2-yl)-5-(3,4-dimethoxyphenyl)-4,5-dihydro-1Hpyrazol-3-yl)phenol(R) | 10–50 | | | | | [38] |
| 4 | (2-(3-(pyridin-2-yl)-5-(3,4,5-trimethoxyphenyl)-4,5-dihydro-1H-pyrazol-1-yl)benzo[d]thiazole (S) | 0–40 | | | | | [39] |
| 5 | 4-(2-(3-Methyl-5-oxo-1-tosyl-1H-pyrazol-4(5H)-ylidene)hydrazinyl)-N-(pyrimidin-2-yl)benzenesulfonamide (T) | 20–100 | 17 | 94.8–97 | 1.3–2.34 | River, ground, and tap water | [2] |
| 6 | coumarin-based pyrazoline | 0–120 | 0.101 | | | Imaging in HeLa cells | [41] |
| 7 | Pyrazole-pyrazoline (U) | 0–10 | .00039 | | | | [40] |
| 8 | 5-(4-methoxyphenyl)-3-(5-methylfuran-2-yl)-1-phenyl-4,5-dihydro-1H-pyrazole (PFM) | 0–3 | 0.12 | 97.2–100 | 0.59–2.03 | Tap, river and sewage waste water | This work |

Conclusions

The synthesized organic fluorescent probe based on pyrazoline 5-(4-methoxyphenyl)-3-(5-methylfuran-2-yl)-1-phenyl-4, 5-dihydro-1H-pyrazole (PFM) has been designed for the selective detection of Fe^{3+} ions. The sensor PFM displayed a “turn off” fluorescence response towards Fe^{3+} ion with a detection limit of 0.12 μM . The binding stoichiometry of Fe^{3+} ions with PFM was 1:1 confirmed by Job’s plot, and their binding mechanism of them was demonstrated by paramagnetic enhanced quenching, FRET and density functional theory (DFT) study. The proposed PFM-sensor was satisfactory applied for quantitative and cost-effective detection of Fe^{3+} with good precision in real samples.

Supplementary Information The online version contains supplementary material available at <https://doi.org/10.1007/s10895-022-03024-y>.

Acknowledgements The authors (PS, SB, IM, MY, and AKM) acknowledge the UGC-SAP and Chemistry Department, Punjabi University, Patiala, for providing lab and instrument facilities.

Authors' Contributions Promila Sharma: Performed the experimentation. Shikha Bhogal, Irshad Mohiuddin: Helped in performing the experiments. Mohammad Yusuf and Ashok Kumar Malik: Helped in writing and supervised the research work.

Funding The authors did not receive support from any organization for the submitted work and have no financial or non-financial interests to disclose.

Availability of Data and Material Data and material information is provided and will be shared on request.

Declarations

Ethics Approval There are no ethics approvals required for this research work.

Consent to Participate All authors will participate in the revision of the manuscript.

Consent for Publication All authors agree for the publication.

Conflicts of Interest/Competing Interests All the authors declare that there is no conflict of interest.

References

- Li C et al (2020) Reaction-based highly selective and sensitive monomer/polymer probes with Schiff base groups for the detection of Hg^{2+} and Fe^{3+} ions. *Spectrochim Acta Part A Mol Biomol Spectrosc* 243:118763
- Sayed A et al (2021) A novel fluorescent sensor for fast and highly selective turn-off detection of Fe^{3+} in water and pharmaceutical samples using synthesized azopyrazole-benzenesulfonamide derivative. *J Mol Struct* 1225:129175

- Wang M, Guo L, Cao D (2017) Porous organic polymer nanotubes as luminescent probe for highly selective and sensitive detection of Fe³⁺. *Sci China Chem* 60(8):1090–1097
- Vanjare BD et al (2018) Discriminating chemosensor for detection of Fe³⁺ in aqueous media by fluorescence quenching methodology. *Bull Korean Chem Soc* 39(5):631–637
- Zhang B et al (2017) A dual-response quinoline-based fluorescent sensor for the detection of Copper (II) and Iron (III) ions in aqueous medium. *Sens Actuators B Chem* 243:765–774
- Rangasamy M, Palaninathan K (2018) A pyrazoline-based fluorescent chemosensor for Al³⁺ ion detection and live cell imaging. *New J Chem* 42(13):10891–10897
- Zhang Y-P et al (2021) Fluorogenic recognition of Zn²⁺, Cd²⁺ by a new Pyrazoline-based Multi-Analyte chemosensor and its application in live cell imaging. *Inorg Chem Commun* 130:108735
- Zhang L et al (2017) High solid fluorescence of a pyrazoline derivative through hydrogen bonding. *Molecules* 22(8):1304
- Varghese B et al (2017) Unveiling a versatile heterocycle: pyrazoline—a review. *RSC Adv* 7(74):46999–47016
- Shaaban MR, Mayhoub AS, Farag AM (2012) Recent advances in the therapeutic applications of pyrazolines. *Expert Opin Ther Pat* 22(3):253–291
- Singh P et al (2018) 2-Pyrazolines as biologically active and fluorescent agents, an overview. *Anti-Cancer Agents Med Chem Formerly Curr Med Chem-Anti-Cancer Agents* 18(10):1366–1385
- Hasan A, Abbas A, Akhtar MN (2011) Synthesis, characterization and fluorescent property evaluation of 1, 3, 5-triaryl-2-pyrazolines. *Molecules* 16(9):7789–7802
- Chibac AL et al (2019) Pyrazoline based chloride sensor for body fluids screening. *J Mol Liq* 284:139–146
- Bozkurt E, Gul HI (2020) Selective fluorometric “Turn-off” sensing for Hg²⁺ with pyrazoline compound and its application in real water sample analysis. *Inorg Chim Acta* 502:119288
- Bozkurt E, Gul HI (2018) A novel pyrazoline-based fluorometric “turn-off” sensing for Hg²⁺. *Sens Actuators B Chem* 255:814–825
- Zhang Y-P et al (2021) A novel pyrazoline-based fluorescent probe for Cu²⁺ in aqueous solution and imaging in live cell. *Inorg Chem Commun* 129:108612
- Sharma P et al (2022) Experimental and Theoretical Studies of the Pyrazoline Derivative 5-(4-methylphenyl)-3-(5-methylfuran-2-yl)-1-phenyl-4, 5-dihydro-1H-Pyrazole and its Application for Selective Detection of Cd²⁺ ion as Fluorescent Sensor. *J Fluoresc* 1–13
- Bhagal S et al (2021) Synchronous Fluorescence Determination of Al³⁺ Using 3-Hydroxy-2-(4-Methoxy Phenyl)-4H-Chromen-4-One as a Fluorescent Probe. *J Fluoresc* 1–9
- Holla BS, Akberali P, Shivananda M (2000) Studies on arylfuran derivatives: Part X. Synthesis and antibacterial properties of arylfuryl- Δ^2 -pyrazolines. *II Farmaco* 55(4):256–263
- Han C et al (2014) Design and synthesis of a highly sensitive “Turn-On” fluorescent organic nanoprobe for iron (iii) detection and imaging. *J Mater Chem C* 2(43):9077–9082
- Chung PK et al (2013) A pyrene-based highly selective turn-on fluorescent chemosensor for iron (iii) ions and its application in living cell imaging. *J Fluoresc* 23(6):1139–1145
- Joshi S et al (2015) Experimental and theoretical study: Determination of dipole moment of synthesized coumarin–triazole derivatives and application as turn off fluorescence sensor: High sensitivity for iron (III) ions. *Sens Actuators B Chem* 220:1266–1278
- Rahaman S et al (2010) Synthesis and antihistaminic activity of novel pyrazoline derivatives. *Int J Chem Tech Res* 2:16–20
- Nisa S, Yusuf M (2020) Synthetic and antimicrobial studies of N-substituted-pyrazoline-based new bisheterocycles. *J Heterocycl Chem* 57(4):2024–2036
- Yang Y-S et al (2022) A novel pyrazoline-based fluorescence probe armed by pyrene and naphthol system for the selective detection of Cu²⁺ and its biological application. *J Iran Chem Soc* 1–11
- Kumar M et al (2018) A selective ‘turn-on’ fluorescent chemosensor for detection of Al³⁺ in aqueous medium: experimental and theoretical studies. *Sens Actuators, B Chem* 260:888–899
- Lu S et al (2017) Near-infrared photoluminescent polymer–carbon nanodots with two-photon fluorescence. *Adv Mater* 29(15):1603443
- Hashemi N et al (2018) Hemoglobin-incorporated iron quantum clusters as a novel fluorometric and colorimetric probe for sensing and cellular imaging of Zn (II) and cysteine. *Microchim Acta* 185(1):1–11
- Udhayakumari D et al (2014) Highly fluorescent probe for copper (II) ion based on commercially available compounds and live cell imaging. *Sens Actuators, B Chem* 198:285–293
- Saravanamoorthy S et al (2021) Molecular Geometry, Vibrational Spectroscopic, Molecular Orbital and Mulliken Charge Analysis of 4-(Carboxyamino)-Benzoic Acid: Molecular Docking and Dft Calculations. Preprints 2021070215. <https://doi.org/10.20944/preprints202107.0215.v1>
- Subashini G et al (2017) Quinoline appended pyrazoline based Ni sensor and its application towards live cell imaging and environmental monitoring. *Sens Actuators B Chem* 243:549–556
- Issa TB et al (2019) Synthesis, crystal structure, DFT calculations and molecular docking of L-pyroglutamic acid. *J Mol Struct* 1178:436–449
- Zuo Z et al (2019) A dual responsive colorimetric/fluorescent turn-on sensor for highly selective, sensitive and fast detection of Fe³⁺ ions and its applications. *J Photochem Photobiol A* 382:111876
- Muthu S, Paulraj EI (2013) Molecular structure and spectroscopic characterization of ethyl 4-aminobenzoate with experimental techniques and DFT quantum chemical calculations. *Spectrochim Acta Part A Mol Biomol Spectrosc* 112:169–181
- Berhanu AL et al (2020) Experimental and theoretical studies of the schiff base (Z)-1-(thiophen-2-yl-methyleneamino) propane-2-ol. *J Mol Struct* 1200:127104
- Hu S et al (2013) A new selective fluorescent sensor for Fe³⁺ based on a pyrazoline derivative. *Spectrochim Acta Part A Mol Biomol Spectrosc* 113:325–331
- Asiri AM et al (2019) Physicochemical and Photophysical investigation of newly synthesized carbazole containing pyrazoline-benzothiazole as fluorescent chemosensor for the detection of Cu²⁺, Fe³⁺ & Fe²⁺ metal ion. *J Mol Struct* 1195:670–680
- Khan SA (2020) Multi-step synthesis, photophysical and physicochemical investigation of novel pyrazoline a heterocyclic D- π -A chromophore as a fluorescent chemosensor for the detection of Fe³⁺ metal ion. *J Mol Struct* 1211:128084
- Asiri AM, Al-Amari MM, Khan SA (2020) Multistep Synthesis and Photophysical Investigation of Novel Pyrazoline, a Heterocyclic D- π -a Chromophore (PTPB) as a Fluorescent Chemosensor for the Detection of Fe³⁺ Metal Ion. *Polycycl Aromat Compd* 1–15
- Zhang Y-P et al (2021) A novel fluorescent probe based on pyrazole-pyrazoline for Fe (III) ions recognition. *J Fluoresc* 31(1):29–38
- Zhang Y-P et al (2021) A novel coumarin-based pyrazoline fluorescent probe for detection of Fe³⁺ and its application in cells. *Inorg Chim Acta* 525:120469

Publisher's Note Springer Nature remains neutral with regard to jurisdictional claims in published maps and institutional affiliations.

Springer Nature or its licensor holds exclusive rights to this article under a publishing agreement with the author(s) or other rightsholder(s); author self-archiving of the accepted manuscript version of this article is solely governed by the terms of such publishing agreement and applicable law.